Li, J.; Tang, J.; Mi, W.; Tian, C.; Emeis, K.; Ebinghaus, R.; Xie, Z. :
Spatial Distribution and Seasonal Variation of Organophosphate Esters in Air above the Bohai and Yellow Seas, China.
In: Environmental Science and Technology. Vol. 52 (2017) 1, 89 - 97.
First published online by ACS: 29.11.2017

https://dx.doi.org/10.1021/acs.est.7b03807

Spatial Distribution and Seasonal Variation of Organophosphate Esters in Air above the Bohai and Yellow Seas, China

Jing Li,[†,⊥] Jianhui Tang,[*,‡] Wenying Mi,[§] Chongguo Tian,[‡] Kay-Christian Emeis,[†,⊥] Ralf Ebinghaus,[†] and Zhiyong Xie[*,†]

[†]Centre for Materials and Coastal Research, Institute of Coastal Research, Helmholtz-Zentrum Geesthacht, Geesthacht 21502, Germany

[‡]Key Laboratory of Coastal Environmental Processes and Ecological Remediation, Yantai Institute of Coastal Zone Research, CAS, Yantai 264003, China

[§]MINJIE Analytical Laboratory, Geesthacht 21502, Germany

[⊥]School of Integrated Climate System Sciences, University of Hamburg, Hamburg 20144, Germany

ABSTRACT: Nine organophosphate esters (OPEs) were investigated in air samples collected over the Bohai and Yellow Seas (East Asia) during a research cruise between June 28 and July 13, 2016.

These same OPEs were quantified at a research site (North Huangcheng Island, NHI) in the middle of the Bohai Strait from May 16, 2015, to March 21, 2016. The median total OPE (ΣOPE) concentration over the Bohai and Yellow Seas was 280 pg/m^3. Tris(1-chloro-2-propyl)(TCPP) was the most abundant OPE, followed by tris(2-chloroethyl) phosphate (TCEP), tri-iso-butyl phosphate (TiBP), and tri-*n*-butyl phosphate (TnBP). Particle-bound OPEs accounted for 51 ± 21% of the total OPEs. On NHI, the median ΣOPE concentration was 210 pg/m^3, and the average particle-bound fraction was 82 ± 17%. For samples collected on NHI, significant negative linear correlations were found between the gaseous OPEs and $1/T$ (T: temperature (K)) (except TDCP, TPeP, and TCP). Among the 79 investigated samples, significant correlations between the measured OPE gas/particle partitioning coefficients ($K_{p,m}$) and subcooled liquid pressure (P_L) ($p < 0.05$) were found for only 14 samples, suggesting that OPEs have low potential to achieve equilibrium or ascribe to the artificial sampling. The annual dry deposition input of OPEs into the Bohai and Yellow Seas is estimated to be 12 tons/year.

INTRODUCTION

Organophosphate esters (OPEs) are commonly used as flame retardants and plasticizers.[1,2] In recent years, global production and usage of OPEs has increased sharply, and from 1992 to 2013, the volume of worldwide OPE consumption increased from 102,000 to 370,000 tons.[3,4] In China, the price of the brominated intermediates has risen continuously since 2005 due to limitations in the supply of bromate.[4] As a result, the market prices for brominated flame retardants (BFRs) are higher than those of flame retardants (FRs) from OPEs.[4] Consequently, the consumption of OPEs increased from 11,000 tons in 1995 to 70,000 tons in 2007 and to 179,000 tons in 2012. Aside from the high OPE consumption, China is also the largest global e-waste importer and recycler.[5] If such recycling is performed improperly (i.e., direct burning), it contributes to the release of chemicals, including OPEs.[6]

The occurrence of atmospheric OPEs has been reported above the European seas,[7,8] the open oceans,[9−11] and the polar regions.[9,12] In East Asia, OPEs have been detected over the South China Sea (nine OPEs; median of total OPEs: 91 pg/m^3),[13] over the East China Sea (four OPEs in one sample; 1066 pg/m^3 in total),[12] and over the Japan Sea (eight OPEs in two samples; 450 and 2900 pg/m^3 in total, respectively).[11] However, no data are available over the Bohai and Yellow Seas, which are influenced by East Asian continental air masses, especially from the east coast of China.

Previous studies focused mainly on OPE in the particulate phase, and only a few papers reported OPE in the gaseous phase. Recently, Wolschke et al. reported that on average 55% of OPEs could be detected in the gaseous phase.[14] Li et al. detected gaseous OPEs in air over the North Atlantic and Arctic (mean fraction of gaseous OPEs: 33 ± 17%).[9] These studies highlighted the importance of the research on OPE gas/particle partitioning, which determines the environmental fate and long-range transport mechanisms of OPEs.

The Bohai Sea is a nearly enclosed interior sea with an area of approximately 78,000 km^2, length of coastline of 3,784 km, and average depth of 18 m.[15] The Yellow Sea, which is nearly surrounded by mainland China and the Korean Peninsula, is at the margin of the western Pacific Ocean and is connected with the Bohai Sea via the Bohai Strait (Figure 1).[16] The Bohai and

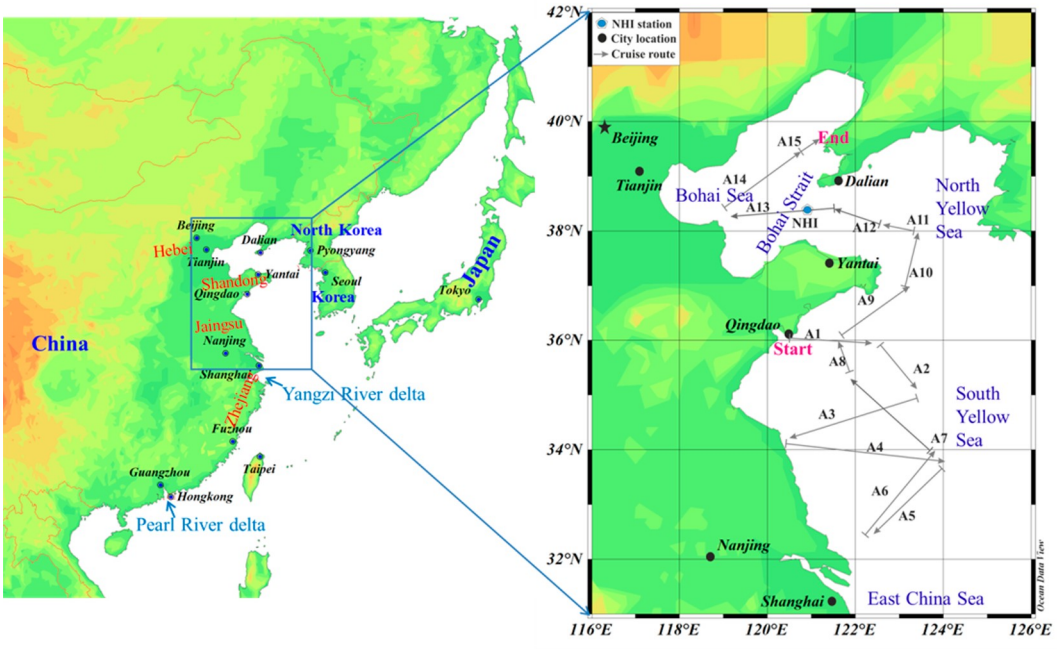

Figure 1. Map of the research area showing the sampling cruise route (gray arrows) and the location of the long-term sampling station at North Huangcheng Island (NHI).

Yellow Seas have a combined total area about 458,000 km^2.[15,17] North Huangcheng Island (NHI) is situated in the center of the Bohai Strait, where the Bohai Sea and Yellow Sea meet (Figure 1).[18] Because NHI has a low population density and high vegetation coverage and is separated from the mainland by 65 km, it is suitable for monitoring baseline pollution and the seasonal variability of OPEs in the region.[18]

This study investigated the annual variability of OPEs in air over NHI and the spatial distribution of OPEs over the Bohai and Yellow Seas. The data are examined to estimate the gas/particle partitioning of OPEs employing the Junge−Pankow adsorption model (J−P model) and the absorption model based on the octanol/air partition coefficient (K_{oa}-based model). Further, atmospheric particle-bound dry deposition of OPEs was calculated with the data measured at the Bohai and Yellow Seas. This work improves understanding of the occurrence and fate of OPEs in the marine environment.

MATERIALS AND METHODS

Sampling Campaign. Fifteen air samples were taken over the Bohai and Yellow Seas during a research cruise between June 28 and July 13, 2016, on the research vessel *Dongfanghong 2* (Figure 1). Eighty-one air samples were collected from NHI between May 16, 2015, and March 21, 2016 (Figure 1). A high-volume air sampler was used to collect the air samples. The details of the sampling procedures were published previously.[9] Briefly, atmospheric particle samples were collected using a glass fiber filter (GFF; pore size: 0.7 μm; diameter: 150 mm), and gaseous phase samples were collected by follow-up PUF/XAD-2 resin column. Prior to deployment, the PUF/XAD-2 columns were cleaned with dichloromethane (DCM), hexane/acetone (1:1$_{V:V}$), and methanol for 16 h each. Prior to deployment, the GFF filters were baked at 450 °C for 12 h to remove organic residue. All solvents were residue grade. Ten field blanks were collected by briefly exposing the columns and filters to the atmosphere at the sampling sites (five for the cruise and five for NHI). Detailed sampling information is presented in Tables S1 and S2.

Sample Analysis. The air sample pretreatment and analysis followed the method published by Xie et al.[19] Briefly, GFFs and PUF/XAD-2 were spiked with 20 ng of d_{12}-TCEP, d_{15}-TPhP, and d_{27}-TnBP as surrogates and extracted with MX-Soxhlet for 16 h using 200 mL of DCM. The GFFs and PUF/XAD-2 were extracted separately. Ten mL of hexane was added to all extracts, followed by a preconcentration to 1 mL by rotary evaporation, and further volume reduction down to 150 μL with a nitrogen evaporator (Barkey GmbH, Germany).[13]C_6-PCB 208 was used as the injection standard.

An Agilent 7890A gas chromatograph coupled to an Agilent 7010A Triple Quadrupole mass spectrometer (GC-MS/MS) and equipped with a programmed temperature vaporizer (PTV) injector (Agilent, USA) was used for analysis. The MS transfer line and the high sensitivity electron impact ionization source (HSEI) were held at 280 and 230 °C, respectively. The MS/MS was operated in Multiple Reaction Monitoring (MRM) mode. Detailed information regarding the GC-MS/MS setup was published previously and is presented in Text S1.[9]

Nine OPEs were analyzed in this work (Table S3): TCPP (tris(1-chloro-2-propyl) phosphate, including three isomers), TCEP (tris(2-chloroethyl) phosphate), TDCP (tris(1,3-dichloro-2-propyl) phosphate), TnBP (tri-*n*-butyl phosphate), TiBP (tri-iso-butyl phosphate), TPhP (triphenyl phosphate), TPeP (tripentyl phosphate), TEHP (tris(2-ethylhexyl) phosphate), and TCP (tricresyl phosphate, including four isomers).

Quality Assurance/Quality Control (QA/QC). Five blanks were collected for the cruise and NHI station, respectively. For the gaseous phase, the lowest absolute blank was detected for TPeP (cruise: 1.4 ± 1.4 pg; NHI: 1.7 ± 1.0 pg), whereas the highest was found for TCPP (cruise: 110 ± 27 pg; NHI: 260 ± 130 pg). For the particulate phase, the absolute blank ranged from 1.2 ± 0.22 pg for TPeP to 380 ± 48 pg for TCP on NHI (cruise: 2.8 ± 1.1 pg for TPeP; 530 ± 88 pg for

TCP; Table S4). The concentrations of field blanks were obtained through absolute blank divided by the sample volume (300 m^3 for the gaseous phase and 150 m^3 for the particulate phase, as only half of each filter was analyzed; Table S5). The OPE concentrations in samples are blank corrected.

The method detection limits (MDLs) were calculated based on field blank concentrations plus three times their standard deviation (3σ). For the Bohai and Yellow Seas, the MDLs were 0.02−0.79 pg/m^3 in the gaseous phase and 0.04−5.3 pg/m^3 in the particulate phase (Table S5). On NHI, the MDLs were 0.02−2.2 pg/m^3 for the gaseous phase and 0.01−5.0 pg/m^3 for the particulate phase (Table S5).

For the gaseous phase, mean recovery rates of the spiked experiments varied between 82 ± 22% (TEHP) and 140 ± 15% (TDCP) (n = 5; Table S6). The analytical method for the particle phase was validated with reference material NIST SRM 2585, which has been suggested by several laboratories, although it is not certified for OPEs. NIST SRM 2585 dust was wrapped in the GFF filters and extracted in the same way as particle samples (results in Table S8). The OPE levels in SRM 2585 were compared with those reported in the literature (Table S9), and similar concentrations were determined for all OPEs except TCEP.[10,20−27] The mean TCEP concentration in this study (1.9 ± 0.15 μg/g) was approximately double that of other reports (0.68−0.88 μg/g, Table S9). The TiBP concentrations (mean: 0.013 ± 0.005 μg/g) were comparable to those reported by Brandsma et al. (on average: 0.017 μg/g)[25] and lower than those reported by Ali et al. (1.6 ± 0.39 μg/g).[22] TPeP was detected in NIST SRM 2585, with a mean concentration of 0.003 ± 0.0001 μg/g. The extraction efficiency was tested by extracting NIST SRM 2585 dust samples twice. The recoveries in the first extraction ranged from 79 ± 4.1% (TEHP) to 99.5 ± 0.15% (TCP; Table S10).

Air Mass Back Trajectories. Air mass back trajectories for the sampling stations were obtained using the NOAA HYSPLIT model.[28] During the Bohai and Yellow Seas sampling cruises, back trajectories were calculated at 10 m above sea level in 6 h increments for each sample for a total of 120 h (Figure S2). For NHI, the cluster-mean trajectories of the four seasons during the sampling period (height: 100 m) are given in Figure S1.

Gas/Particle Partitioning Methods. The particle-bound fractions measured in this study (φ_m) were calculated from the following equation based on C_p (OPE concentration in the particulate phase, pg/m^3) and C_g (OPE concentration in the gaseous phase, pg/m^3):

$$\varphi_m = \frac{C_p}{C_p + C_g} \quad (1)$$

The measured partitioning coefficient $K_{p,m}$ can be calculated by[29]

$$K_{p,m} = \frac{C_p/C_{TSP}}{C_g} \quad (2)$$

where C_{TSP} is the total suspended particle concentration (μg/m^3).

The subcooled vapor pressure P_L° is an important factor for the gas/particle partitioning of organic compounds. Generally, a highly correlated linear regression can be obtained between log $K_{p,m}$ and log P_L° for given samples for a group of compounds[29]

$$\log K_{p,m} = m \log p_L^\circ + b \quad (3)$$

where the slope m and intercept b are fitting constants. At the ideal equilibrium, the slope m should be close to −1. In this study, the linear relation between log $K_{p,m}$ and log P_L° was investigated for each sample on NHI. Temperature-dependent P_L° values for TCEP, TCPP, TDCP, TPhP, and TEHP were estimated according to the equations reported by Brommer et al.[30] For the other four OPEs, the vapor pressures were obtained from EPI Suite 4.1.

Two prediction models were adopted in this study, the J−P model and the K_{oa}-based model. The J−P model, proposed by Pankow in 1987, is based on P_L°.[31] The particle-bound fraction φ_{J-P} of a target compound is estimated by[31]

$$\varphi_{J-P} = \frac{c\theta}{p_L^\circ + c\theta} \quad (4)$$

where c is a constant that depends on the properties of the substance, and θ is the surface area of particle per unit volume of air (cm^2/cm^3). This study assumes c to be 17.2 Pa cm for OPEs[32] and θ to be 1.0×10^{-6} for rural air.[33]

The predicted gas/particle partitioning coefficient $K_{p,koa}$ through the K_{oa}-based model is (details in Text S2)[34]

$$K_{p,koa} = \log K_{oa} + \log f_{OM} - 11.9 \quad (5)$$

where f_{OM} is the fraction of organic matter (OM) phase in the aerosol (f_{OM} was assumed as 0.1). The temperature-dependent log K_{oa} values were obtained from the report of Wang et al.[35]

The field predicted particle-bound fraction based on the K_{oa}-based model (φ_{koa}) can be calculated from the following equation:[31]

$$\varphi_{koa} = \frac{K_{p,koa}C_{TSP}}{K_{p,koa}C_{TSP} + 1} \quad (6)$$

Statistical Analysis. The Spearman's correlation coefficient was used to evaluate the correlations (by SPSS 20), because the data set was not normally distributed. Linear regression was performed with Excel 2016. The nonparametric ANOVA test (Kruskal−Wallis Test) coupled with the Dunn posthoc test (by GraphPad InStat 3.10) were adopted to analyze significant differences of OPE levels between the four seasons. The value of 0.05 was used as the p-value to determine statistical significance. Concentrations below the MDLs were replaced by 2/3 of the MDL for the statistical analysis. As a nonparametric test was conducted in this study, outliers were included. The outliers that were excluded for the regression are explained in the corresponding text.

RESULTS AND DISCUSSION

OPE Concentrations over the Bohai and Yellow Seas.

All targeted OPEs except TEHP (93%) and TCP (73%) were detected in all air samples (gaseous and particulate phases). The sum of the nine OPE concentrations (ΣOPE) ranged from 100 to 750 pg/m^3 (median: 280 pg/m^3). The three chlorinated OPEs accounted for 66 ± 15% of the total OPEs, and the remainder was composed of the six nonchlorinated OPEs (34 ± 15%). TCPP was the most abundant OPE (range: 43−530 pg/m^3; median: 100 pg/m^3), followed by TCEP (range: 27−150 pg/m^3; median: 71 pg/m^3), TiBP (range: 19−210 pg/m^3; median: 57 pg/m^3), and TnBP (range: 5.0−37 pg/m^3; median: 13 pg/m^3). The details of the individual OPE concentrations

are summarized in Table 1. The composition profiles of the OPEs are shown in Figure S3.

In the gaseous phase, the ΣOPE concentrations ranged from 2.3 to 270 pg/m^3 (median: 170 pg/m^3), and these were dominated by three OPEs, TiBP, TCPP, and TCEP, which contributed 32 ± 18%, 27 ± 15%, and 25 ± 11% to ΣOPEs, respectively. In the particulate phase, the ΣOPE concentrations ranged from 44 to 520 pg/m^3 (median: 150 pg/m^3), with a predominance of TCPP (50 ± 11% of ΣOPEs), followed by TCEP (25 ± 7%) and TiBP (14 ± 12%).

OPE Concentrations on NHI. Most of the nine OPEs were detected in all samples, but TDCP and TCP were detected in 98% and 75% of the total samples, respectively. The ΣOPE concentrations ranged from 36 to 1600 pg/m^3 (median: 210 pg/m^3) which is comparable to the values measured in marine air above the Bohai and Yellow Seas detected during the ship expedition. The mean concentrations of the major OPEs detected on NHI were (in decreasing order): TCEP (median: 77 pg/m^3) > TCPP (29 pg/m^3) ≈ TiBP (28 pg/m^3) > TPhP (18 pg/m^3) > TnBP (12 pg/m^3; Table 1). The chlorinated OPEs accounted for 55 ± 16% of the total OPEs.

In the gaseous phase, the ΣOPE concentrations ranged from 1.2 to 360 pg/m^3 (median: 31 pg/m^3), which is lower than ΣOPE levels in the particulate phase (range: 5.0 to 1500 pg/m^3, median: 170 pg/m^3). Similar patterns were found for OPEs between the gaseous and the particle phases, with TCEP being the most abundant OPE (gaseous phase: 31%; particulate phase: 38%), followed by TiBP, TCPP, TPhP, and TnBP.

Most previous studies analyzed particle-bound OPEs. Therefore, the OPE levels in the particulate and gaseous phases were compared separately with those reported in the literature. The total and individual OPE concentrations in the particulate phase were generally in the low range of OPE levels reported for most oceanic atmosphere and remote sites (Table S11). Concentration of total OPE reported for one sample collected over the East China Sea in October 2009 was 1100 pg/m^3 (four OPEs)[12] and thus approximately six times higher than in this study (nine OPEs; median: 150 pg/m^3). The higher OPE levels in the East China Sea likely reflect the influence of the Yangzi River Delta region (Figure 1), a major production region for OPEs.[4] Two samples taken over the Sea of Japan had total OPE levels (eight OPEs) of 450 pg/m^3 and 2900 pg/m^3, respectively.[11] The author argued that the high concentration (2900 pg/m^3) signals continental air from Asia. In the South China Sea, lower concentrations (eight OPEs; median: 91 pg/m^3)[13] were found than in this work. Furthermore, the median of the ΣOPE levels in this study (150 pg/m^3) was two times higher than that reported from the North Atlantic and Arctic (eight OPEs; median: 48 pg/m^3)[9] but similar to that measured near the Antarctic Peninsula (four OPEs; median: 141 pg/m^3; Table S11).[12] It was lower than that reported from the North Sea (eight OPEs; median: 281 pg/m^3)[7], the Canadian Arctic (median ship-based: 237 pg/m^3);[36] and in Longyearbyen (334 pg/m^3).[37] Compared to the Mediterranean Sea (14 OPEs; median: ~1,455 pg/m^3; Table S11),[8] the Black Sea (14 OPEs; median: 2,006 pg/m^3),[8] and concentrations reported from open oceans as reported by Castro-Jimenez et al. (nine OPEs; median range: 1,500−2,200 pg/m^3),[10] the median found in Bohai and Yellow Sea is 1 order of magnitude lower (Table S11).

Several papers have reported OPE levels in the gaseous phase, such as OPEs in the North Sea (eight OPEs; median: 54 pg/m^3) and the North Atlantic and Arctic (eight OPEs;

Table 1. Range, Mean ± Standard Deviation, and Median of Individual OPE Concentrations in Air (pg/m^3) above the Bohai and Yellow Seas and North Huangcheng Island (NHI)

	Bohai and Yellow Seas (n = 15)						North Huangcheng Island (n = 81)					
	gaseous phase			particulate phase			gaseous phase			particulate phase		
OPE (pg/m^3)	range	mean	median	range	mean	median	range	mean	median	range	mean	median
TCPP	n.d.−130	45 ± 35	42	19−390	86 ± 88	66	0.2−26	5.6 ± 5.6	3.2	n.d.−160	34 ± 33	26
TCEP	n.d.−73	38 ± 18	38	14−94	38 ± 23	28	0.69−120	14 ± 17	10	0.40−1000	100 ± 170	63
TDCP	n.d.−4.3	0.81 ± 1.0	0.57	0.75−13	4.5 ± 3.1	4.6	n.d.−2.6	0.35 ± 0.61	n.d.	n.d.−80	7.1 ± 11	3.8
TiBP	0.30−170	54 ± 50	30	2.3−95	24 ± 29	12	n.d.−82	8.1 ± 12	4.8	1.0−164	33 ± 29	24
TnBP	0.46−36	8.9 ± 8.7	8.0	1.2−14	4.8 ± 3.6	4.6	n.d.−190	11 ± 28	2.7	n.d.−1100	61 ± 180	8.2
TPeP	0.03−1.2	0.43 ± 0.38	0.27	0.04−0.30	0.13 ± 0.08	0.10	n.d.−0.41	0. 05 ± 0.07	0.03	0.01−2.4	0.24 ± 0.31	0.16
TPhP	0.19−4.7	2.0 ± 1.2	1.7	1.4−15	5.0 ± 4.0	2.8	0.17−22	4.4 ± 4.3	2.7	n.d.−110	22 ± 25	11
TEHP	n.d.−5.3	1.6 ± 1.4	1.0	n.d.−8.5	1.8 ± 2.5	1.8	n.d.−30	2.3 ± 4.4	1.1	n.d.−180	10 ± 30	1.5
TCP	n.d.−5.2	1.7 ± 1.7	1.6	n.d.−26	2.6 ± 7.0	n.d.	n.d.−7.1	0.60 ± 1.4	n.d.	n.d.−18	1.7 ± 3.1	0.35
ΣOPEs	2.3−270	150 ± 77	170	44−520	170 ± 120	150	1.2−360	47 ± 54	31	5.0−1500	270 ± 300	170

median: 17 pg/m^3; Table S12), which are both lower than those of the Bohai and Yellow Seas (eight OPEs; median: 170 pg/m^3). However, the concentrations found at NHI (median: 31 pg/m^3) are similar to those from the literature. The difference of OPE levels between samples from the NHI and the Bohai and Yellow Seas is caused by the variance of distribution in the gaseous and particulate phases, as discussed in the section *Measured Particle-Bound Fractions* below.

To provide an overall perspective of particle-bound OPE levels in global oceanic and remote regions, seven widely measured OPEs, including three chlorinated OPEs (TCEP, TCPP, TDCP) and four nonchlorinated OPEs (TiBP, TnBP, TEHP, TPhP), were chosen for a statistical evaluation (data sourced from the literature and this study). From the 27 regions listed in Table S11, 21 regions, in which at least five of the seven OPEs were detected, were selected for the analysis. Data for the Canadian Arctic (land-based) were not included, because TnBP was only analyzed at Resolute Bay and showed quite high concentrations (median: 416 pg/m^3) compared with other OPEs. According to the statistical results, the chlorinated OPEs accounted for 50% to 96% of the total seven OPEs (median: 76%, Table S13), and the four nonchlorinated OPEs contributed 3.7% to 50% of the total OPEs (median: 24%, Table S13). Among the chlorinated OPEs, the fractions of TCPP (median: 39%, Table S13) and TCEP (median: 24%, Table S13) were higher than the fraction of TDCP (median: 4.2%, Table S13); however, the contributions of the four nonchlorinated OPEs were similar (median: TnBP: 7.6%, TiBP: 4.7%, TEHP: 3.7%, TPhP: 3.0%; Table S13).

Spatial Distribution of OPEs. The highest ΣOPE concentration was observed in Sample A1, which was influenced by air masses that originated from the southern Yellow Sea and passed through the coast of Jiangsu before being collected (Figures 2 and S2). The lowest ΣOPE concentration was found in Sample A9, and the source of the air masses was tracked to the Pacific Ocean (Figures 2 and S2). FRs production in China is generally distributed in the Yangtze River and Pearl River Deltas (Figure 1), where the Jiangsu and Zhejiang regions mainly produce OPE-based FRs.[4] Therefore, it is likely that Jiangsu was the primary source of the OPEs measured in Sample A1.

For Samples A1 to A10, transported by air masses that came mainly from the Pacific Ocean and passed partly though the coastal region of China (Yangzi River Delta and Jiangsu Provinces), the dominant OPE was TCPP (mean: 45 ± 10% of total OPEs). For Samples A11 to A14, for which the air masses passed through the west coast of South Korea and the continent (Samples A12−14) or coast (Sample A11) of Shandong Province (Figure S2) before collection, TiBP was the most abundant OPE (mean: 42 ± 3% of total OPEs). For Sample A15, the dominant OPEs were TiBP and TCPP, which accounted for 42% and 39% of the total OPEs, respectively. All air masses of Sample A15 had finally passed over the northern Bohai Sea region, although they were of different origin (Russia, Mongolia, and China), indicating that this area may be a source region of OPEs.

Seasonal Variation of OPEs. There was no significant difference of ΣOPE concentrations (gaseous and particulate phases) between the different seasons. The median levels were approximately 200 pg/m^3 (summer: 220 pg/m^3; winter: 190 pg/m^3; autumn: 210 pg/m^3; spring: 200 pg/m^3; Figure 3). This phenomenon is a result of the similar particle-bound ΣOPE levels in the four seasons, because the particle-bound OPEs

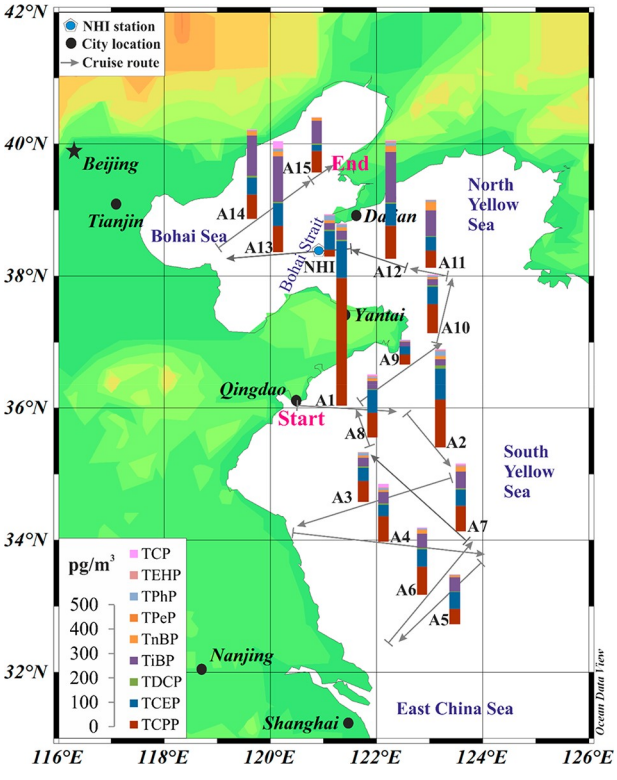

Figure 2. Spatial distribution of OPEs over the Bohai and Yellow Seas and median OPE concentrations at North Huangcheng Island (NHI).

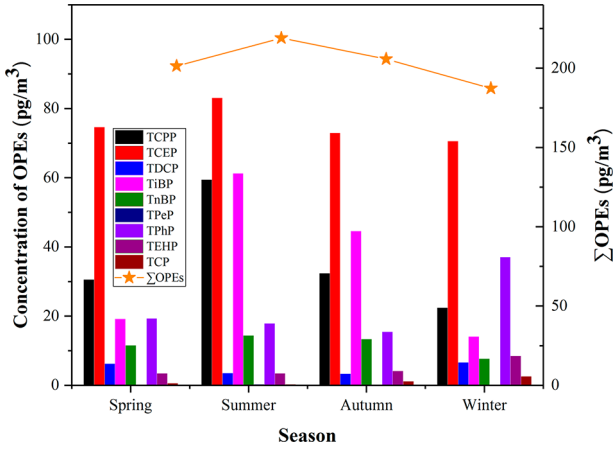

Figure 3. Seasonal variation of individual OPE and ΣOPE concentrations in air at North Huangcheng Island (NHI). The figure shows median values.

accounted for 82 ± 17% of the total OPEs in air (gaseous and particulate phases). In only the gaseous phase, significantly higher concentrations of ΣOPEs and individual OPEs ($p < 0.05$) were measured in summer than in winter (TDCP and TCP were not included because these have low detectability in the gaseous phase, ~30%). A significantly negative correlation ($p < 0.02$) exists between C_g and $1/T$ of most OPEs except TDCP, TPeP, and TCP (Table S14, Figure S4). Relative humidity (RH) had a positive influence on the gaseous OPEs ($p < 0.05$, Table S15), which is consistent with the finding that water hinders degradation of OPEs in air.[38] For the particulate phase, higher concentrations of TCPP and TiBP were observed in summer than in winter, opposite to TPhP and TEHP ($p < 0.05$). C_{TSP}, RH, and temperature had little effect on the

seasonal variance of particle-bound OPEs according to the correlation analysis (Table S16). This result suggests that the seasonal variation patterns of particle-bound OPEs are more indicative of varying air mass origin than the ambient environmental conditions. In winter, the air masses originated mainly from northern China (65% from Mongolia and Russia, 35% from the Hebei and Shandong Provinces), but in summer, oceanic air masses were the dominant source (64% from the Yellow Sea, 19% from the Hebei and Tianjin Provinces; Figure S1). As for spring and autumn, no clear distinction between air mass origins was evident, and both continental and oceanic air masses were main sources. The air masses that originated from the ocean may have passed by the industrial region of the Yangzi River Delta region (Figure 1), which accounts for the high levels of particle-bound TiBP and TCPP as well as the gaseous OPEs in summer.

Measured Particle-Bound Fractions of OPEs. Over the Bohai and Yellow Seas, particle-bound OPEs composed on average 51 ± 21% of the total OPEs. The mean particle-bound fractions of the four major OPEs were in the order of TCPP (63 ± 19%) > TCEP (51 ± 19%) > TnBP (47 ± 23%) > TiBP (30 ± 25%; Figure S4).

On NHI, particle-bound OPEs composed an average 82 ± 17% of the total OPEs, with four major OPEs in the order of TCPP (83 ± 17%) ≈ TCEP (83 ± 16%) > TiBP (82 ± 16%) > TnBP (72 ± 24%; Figure S5).

The particle-bound fractions of ship samples and NHI station samples differed. Over the Bohai and Yellow Seas, OPEs distributed evenly in both gaseous and particulate phases, whereas on NHI OPEs were mainly in the particulate phase. Several factors may be responsible for this different behavior. First, RH is an important factor. Li et al. found that water inhibits the ·OH-initiated degradation of TCPP, which increases the lifetime of gaseous TCPP from the calculated 1.7 h to 0.5−20.2 days.[38] The RH during the ship cruise ranged from 81% to 97% (median: 88%), which was in the upper part of the range at NHI (range: 30−94%; median: 67%). Second, the sampling height on the ship was ∼10 m, which was lower than that on NHI (∼100 m). OPEs have the potential to volatilize from seawater into the air, as demonstrated for the North Atlantic and Arctic.[9] Thus, more gaseous OPEs are expected closer to the surface of the sea. In addition, different air masses also account for the variation of the fractions, as was discussed in sections *Spatial Distribution of OPEs* and *Seasonal Variation of OPEs* above.

On NHI, significantly higher particle-bound fractions of ΣOPEs and individual OPEs were found in winter than in summer. This is likely to reflect low temperature and RH in winter, because significant negative correlations were found between the fractions and temperature ($p < 0.02$; Table S17), as well as with RH ($p < 0.02$; Table S17). In addition, significant positive correlations were observed for OPE fractions and C_{TSP} ($p < 0.002$; Table S17) except for TPeP ($p = 0.94$), indicating that C_{TSP} also contributed the variance of distribution between gaseous and particulate phases.

Previous studies have reported OPE particle-bound fractions in air. Möller et al. detected a mean fraction of 86 ± 25% for the North Sea in 2011.[7] Lower levels were found at the German coast in 2016 (45% on average), which was ascribed mainly to the improved method, as described in the report.[9] Over the North Atlantic and Arctic (2017), the mean fraction was 67 ± 17%.[9] In our study, particle-bound OPEs contributed to 51 ± 21% of total OPEs in ship samples and 82 ± 17% in NHI samples. According to the data reported in the literature and this study, the gas/particle partitioning of OPEs showed a large variation in air samples. Many factors might be responsible for this result, such as C_{TSP}, temperature, RH, and air mass sources as mentioned above, as well as the analytical methodology as reported by Wolschke et al.[9]

Gas/Particle Partitioning Prediction. OPEs can be detected in both the particulate and gaseous phases, and it is important to know how they partition between the two phases in the atmosphere, which can affect the fate and long-range transport of OPEs in the environment. The 81 samples obtained on NHI were used for gas/particle partitioning prediction, with the ranges of temperature, RH, and C_{TSP} being −4 to 27 °C, 30% to 94%, and 16 to 240 μg/m^3, respectively. Only the OPEs that were detectable in both the gaseous and particulate phases in a given sample were included.

Significant correlations between log $K_{p,m}$ and $1/T$ (K^{-1}) were found for TCEP, TiBP, TnBP, TPhP, and TEHP ($p < 0.05$; Table S18, Figure S6). The r^2 values for TCEP, TPhP, and TEHP were >0.40, but the values for TiBP (0.08) and TnBP (0.05) were very low. The regression slopes were positive, showing that $K_{p,m}$ decreased with increasing temperature.

Among the 79 samples investigated (two samples were excluded because of a lack of C_{TSP} data), significant correlations between log $K_{p,m}$ and log P°_{L} of OPE congeners were found for only 14 samples ($p < 0.05$; Table S19). This result suggests that OPEs have low potential to achieve equilibrium or ascribe to the artificial sampling, and the gas/particle partitioning of polar compounds such as OPEs is more complex than the partitioning of nonpolar chemicals.

As log $K_{p,m}$ was correlated with $1/T$ (K^{-1}) for TCEP, TPhP, and TEHP ($p < 0.05$; $r^2 > 0.40$), prediction of their gas/particle partitioning was conducted using the J−P and the K_{oa}-based models. Significant regressed correlations were found between the predicted and measured particle-bound fractions for these three OPEs ($p < 0.01$; r^2 range: 0.23−0.61, Table S20). However, TCEP was predicted to be mainly in the gaseous phase (>95%), which was contrary with the measured data. This discrepancy might result from TCEP strongly absorbed to particles and/or glass fiber filter used for air sampling, which was suggested by Brommer et al.[30] For TEHP and TPhP, the predictions were closer to the measurements than for TCEP (Figure 4), with the ratios of measured to predicted fractions being close to 1 (Table S20). Both the J−P and K_{oa}-based models performed well for TEHP when log $K_{oa} > 12$ (Figure 4b), while they were overestimating the particle-bound fractions when log $K_{oa} < 12$ (Figure 4b). TEHP tends to be in the particulate phase when log $K_{oa} > 13$, while it was in the gaseous phase when log $K_{oa} < 12$. For TPhP, both models underestimate the particle-bound fractions (Figure 4a). The measured data show that approximately 100% of TPhP partitions into the particulate phase when log $K_{oa} > 12$, while the variance increased at log $K_{oa} < 12$ (range: 30% to 99%). The varying partitioning behaviors under similar log K_{oa} values for TPhP may reflect the different environmental conditions, such as the variation of RH, C_{TSP}, and degradation rate of gaseous OPEs. In addition, the nonexchangeability might also contribute to this result, due to the polarity and low volatility of OPEs.

Dry Deposition Flux into the Bohai and Yellow Seas. The deposition flux F_d (ng/m^2/day) is the product of C_p (ng/m^3, OPE concentration in particulate phase) and V_d (m/day, deposition velocity). As there is no field measured V_d for OPEs

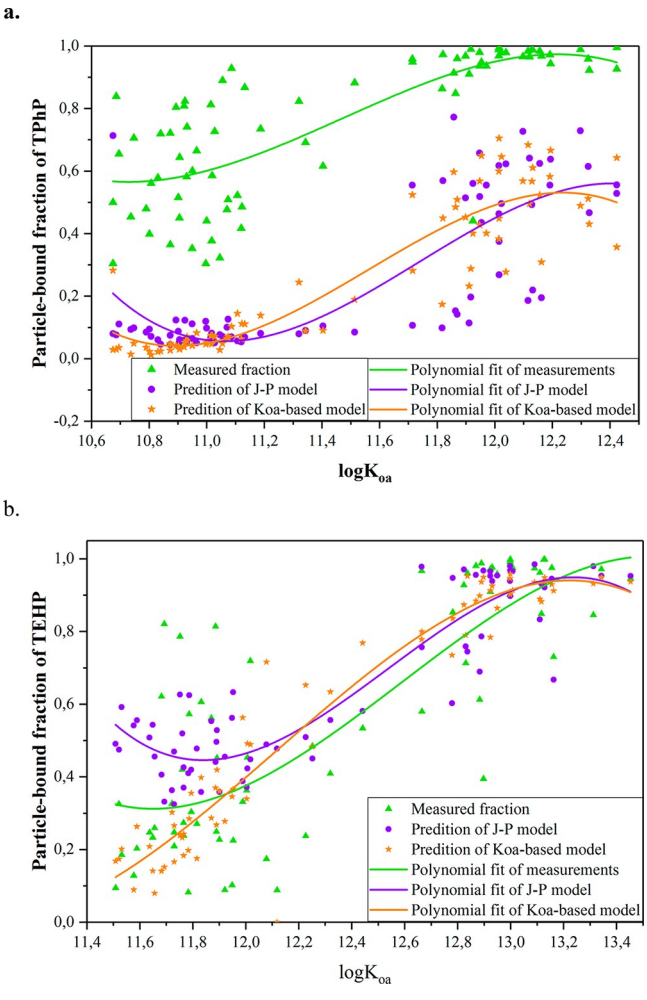

Figure 4. a. Comparison of predicted and measured particle-bound fractions of TPhP (for each sample). b. Comparison of predicted and measured particle-bound fractions of TEHP (for each sample).

or other families of compounds in the Bohai and Yellow Seas, a value of 0.55 cm/s (475.2 m/day) was used for V_d in the present work, which was suggested previously for pollutants over the Yellow Sea.[39] The lack of measured OPE dry deposition velocities results in uncertainties in the estimation of deposition fluxes. The adsorption, desorption, and temperature change during the sampling introduces uncertainties. In addition, breakthrough of target compounds to the vapor phase would affect the concentrations of gaseous OPEs.[9] All of these factors may lead to an over- or underestimation of the dry deposition fluxes.

The ΣOPE dry deposition into the Bohai and Yellow Seas ranged from 21 to 250 ng/m²/day (median: 70 ng/m²/day) and was dominated by TCPP (median: 31 ng/m²/day), followed by TCEP (13 ng/m²/day), TiBP (5.6 ng/m²/day), and TnBP (2.2 ng/m²/day; Figure 5).

On NHI, the median deposition flux was estimated as 79 ng/m²/day. The individual fluxes were in the order of TCEP (30 ng/m²/day) > TCPP (13 ng/m²/day) ≈ TiBP (12 ng/m²/day) > TnBP (4.0 ng/m²/day; Figure 5).

The ΣOPE deposition fluxes into the Bohai and Yellow Seas (median: 70 ng/m²/day) were higher than those published for the South China Sea (16.3 ± 6.7 ng/m²/day)[13] and the North Atlantic and Arctic Oceans (5 ± 4 ng/m²/day).[9] They were similar to those estimated for deposition over in the North Sea

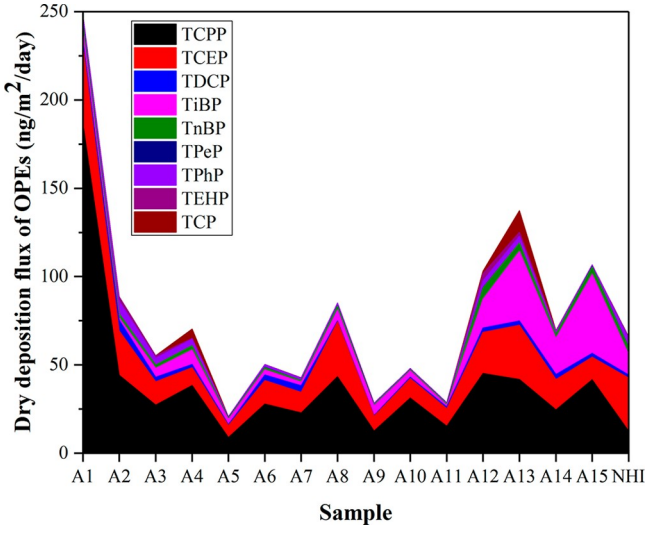

Figure 5. Dry deposition fluxes of OPEs into the Bohai and Yellow Seas at each sample and median fluxes onto North Huangcheng Island (NHI).

(9−240 ng/m²/day),[7] much lower than those over the Mediterranean Sea (70−880 ng/m²/day),[8] and the Black Sea (300−1060 ng/m²/day).[8]

Considering the combined surface area of 458,000 km² of the Bohai and Yellow Seas, the annual OPE input from dry deposition is estimated to be 12 tons/year (median flux: 70 ng/m²/day; Samples A1−A15 and NHI).[15,17] This annual OPE input is 1 order of magnitude lower than that into the Black Sea (~50−170 tons/year), which has a similar surface area (440,000 km²). For only the Bohai Sea, the estimated atmospheric flux was 2.2 tons/year (area: 78,000 km², median flux: 79 ng/m²/day; Samples A14, A15, and NHI), which is higher than that of the German North Sea (area: 42,000 km²; mean flux: 0.71 ± 0.58 tons/year).[7] The annual atmospheric OPE input into the Bohai Sea was ~6 times lower than the riverine input (16 ± 3.2 tons/year; 40 major rivers involved).[40] However, atmospheric transport can lead to faster and larger spatial distribution of OPEs and transports OPEs to the remote ocean.

AUTHOR INFORMATION

Corresponding Authors

*Phone: +86-535-2109151. Fax: +86-535-2109000. E-mail: jhtang@yic.ac.cn.

*Phone: +49-4152-872330. Fax: +49-4152-872332. E-mail: zhiyong.xie@hzg.de.

ORCID

Jing Li: 0000-0003-0187-9179

Jianhui Tang: 0000-0002-9006-263X

Chongguo Tian: 0000-0001-6058-9353

Zhiyong Xie: 0000-0001-8997-3930

NOTES

The authors declare no competing financial interest.

ACKNOWLEDGMENTS

This study was supported by the Chinese Academy of Sciences (2013T2Z0032, KZZD-EW-14, 13337KYSB20130013, 4177338, and XDA11020401), and Bundesministerium für Bildung und Forschung (03F0786C). We are grateful for the field assistant from the crew of Research Vessel *Dongfanghong 2* of the Ocean University of China. J.L. gratefully acknowledges the China Scholarship Council.

REFERENCES

(1) Marklund, A.; Andersson, B.; Haglund, P. Traffic as a source of organophosphorus flame retardants and plasticizers in snow. *Environ. Sci. Technol.* 2005, *39* (10), 3555−3562.

(2) Reemtsma, T.; Quintana, J. B.; Rodil, R.; Garcia-Lopez, M.; Rodriguez, I. Organophosphorus flame retardants and plasticizers in water and air I. Occurrence and fate. *TrAC, Trends Anal. Chem.* 2008, *27* (9), 727−737.

(3) Hartmann, P. C.; Burgi, D.; Giger, W. Organophosphate flame retardants and plasticizers in indoor air. *Chemosphere* 2004, *57* (8), 781−787.

(4) Zhang, Y. Global market analysis of flame retardant (in Chinese with English abstract). *Fine and Specialty Chem.* 2014, *22* (8), 20−24.

(5) Zhang, K.; Schnoor, J. L.; Zeng, E. Y. E-Waste recycling: Where does it go from here? *Environ. Sci. Technol.* 2012, *46*, 10861−10867.

(6) Matsukami, H.; Tue, N. M.; Suzuki, G.; Someya, M.; Tuyen, L. H.; Viet, P. H.; Takahashi, S.; Tanabe, S.; Takigami, H. Flame retardant emission from e-waste recycling operation in northern Vietnam: Environmental occurrence of emerging organophosphorus esters used as alternatives for PBDEs. *Sci. Total Environ.* 2015, *514*, 492−499.

(7) Möller, A.; Xie, Z. Y.; Caba, A.; Sturm, R.; Ebinghaus, R. Organophosphorus flame retardants and plasticizers in the atmosphere of the North Sea. *Environ. Pollut.* 2011, *159* (12), 3660−3665.

(8) Castro-Jimenez, J.; Berrojalbiz, N.; Pizarro, M.; Dachs, J. Organophosphate Ester (OPE) Flame Retardants and Plasticizers in the Open Mediterranean and Black Seas Atmosphere. *Environ. Sci. Technol.* 2014, *48* (6), 3203−3209.

(9) Li, J.; Xie, Z.; Mi, W.; Lai, S.; Tian, C.; Emeis, K.-C.; Ebinghaus, R. Organophosphate Esters in Air, Snow and Seawater in the North Atlantic and the Arctic. *Environ. Sci. Technol.* 2017, *51*, 6887−6896.

(10) Castro-Jimenez, J.; Gonzalez-Gaya, B.; Pizarro, M.; Casal, P.; Pizarro-Alvarez, C.; Dachs, J. Organophosphate Ester Flame Retardants and Plasticizers in the Global Oceanic Atmosphere. *Environ. Sci. Technol.* 2016, *50* (23), 12831−12839.

(11) Möller, A.; Sturm, R.; Xie, Z. Y.; Cai, M. H.; He, J. F.; Ebinghaus, R. Organophosphorus Flame Retardants and Plasticizers in Airborne Particles over the Northern Pacific and Indian Ocean toward the Polar Regions: Evidence for Global Occurrence. *Environ. Sci. Technol.* 2012, *46* (6), 3127−3134.

(12) Cheng, W. H.; Xie, Z. Q.; Blais, J. M.; Zhang, P. F.; Li, M.; Yang, C. Y.; Huang, W.; Ding, R.; Sun, L. G. Organophosphorus esters in the oceans and possible relation with ocean gyres. *Environ. Pollut.* 2013, *180*, 159−164.

(13) Lai, S.; Xie, Z.; Song, T.; Tang, J.; Zhang, Y.; Mi, W.; Peng, J.; Zhao, Y.; Zou, S.; Ebinghaus, R. Occurrence and dry deposition of organophosphate esters in atmospheric particles over the northern South China Sea. *Chemosphere* 2015, *127*, 195−200.

(14) Wolschke, H.; Sühring, R.; Mi, W. Y.; Möller, A.; Xie, Z. Y.; Ebinghaus, R. Atmospheric occurrence and fate of organophosphorus flame retardants and plasticizer at the German coast. *Atmos. Environ.* 2016, *137*, 1−5.

(15) Zhang, Z. H.; Zhu, M. Y.; Wang, Z. L.; Wang, J. Monitoring and managing pollution load in Bohai Sea, PR China. *Ocean Coast. Manage.* 2006, *49* (9−10), 706−716.

(16) Hwang, J. H.; Van, S. P.; Choi, B. J.; Chang, Y. S.; Kim, Y. H. The physical processes in the Yellow Sea. *Ocean Coast. Manage.* 2014, *102*, 449−457.

(17) Jiang, X.; Teng, A. K.; Xu, W. Z.; Liu, X. S. Distribution and pollution assessment of heavy metals in surface sediments in the Yellow Sea. *Mar. Pollut. Bull.* 2014, *83* (1), 366−375.

(18) Liu, Y.; Li, Y.; Chen, J. Research on Modes of Cargo Ro-Ro, Drop and Pull Transport in Land-Sea Transportation Channel between Shandong and Liaoning. *J. Service Sci. Manage.* 2015, *8* (02), 229.

(19) Xie, Z. Y.; Ebinghaus, R. Analytical methods for the determination of emerging organic contaminants in the atmosphere. *Anal. Chim. Acta* 2008, *610* (2), 156−178.

(20) Fan, X.; Kubwabo, C.; Rasmussen, P. E.; Wu, F. Simultaneous determination of thirteen organophosphate esters in settled indoor house dust and a comparison between two sampling techniques. *Sci. Total Environ.* 2014, *491−492*, 80−6.

(21) van den Eede, N.; Dirtu, A. C.; Neels, H.; Covaci, A. Analytical developments and preliminary assessment of human exposure to organophosphate flame retardants from indoor dust. *Environ. Int.* 2011, *37* (2), 454−461.

(22) Ali, N.; Dirtu, A. C.; Van den Eede, N.; Goosey, E.; Harrad, S.; Neels, H.; t Mannetje, A.; Coakley, J.; Douwes, J.; Covaci, A. Occurrence of alternative flame retardants in indoor dust from New Zealand: indoor sources and human exposure assessment. *Chemosphere* 2012, *88* (11), 1276−82.

(23) Bergh, C.; Luongo, G.; Wise, S.; Ostman, C. Organophosphate and phthalate esters in standard reference material 2585 organic contaminants in house dust. *Anal. Bioanal. Chem.* 2012, *402* (1), 51−59.

(24) Van den Eede, N.; Dirtu, A. C.; Ali, N.; Neels, H.; Covaci, A. Multi-residue method for the determination of brominated and organophosphate flame retardants in indoor dust. *Talanta* 2012, *89* (Supplement C), 292−300.

(25) Brandsma, S. H.; de Boer, J.; Cofino, W. P.; Covaci, A.; Leonards, P. E. G. Organophosphorus flame-retardant and plasticizer analysis, including recommendations from the first worldwide interlaboratory study. *TrAC, Trends Anal. Chem.* 2013, *43*, 217−228.

(26) Cristale, J.; Lacorte, S. Development and validation of a multiresidue method for the analysis of polybrominated diphenyl ethers, new brominated and organophosphorus flame retardants in sediment, sludge and dust. *J. Chromatogr. A* 2013, *1305*, 267−75.

(27) Ionas, A. C.; Covaci, A. Simplifying multi-residue analysis of flame retardants in indoor dust. *Int. J. Environ. Anal. Chem.* 2013, *93* (10), 1074−1083.

(28) Draxler, R. R.; Hess, G. *Description of the HYSPLIT4 modeling system*; NOAA Technical Memorandum ERL ARL-224; NOAA Air Resources Laboratory: Silver Spring, MD, 1997; pp 1−24.

(29) Pankow, J. F.; Bidleman, T. F. Interdependence of the Slopes and Intercepts from Log Log Correlations of Measured Gas Particle Partitioning and Vapor-Pressure 0.1. Theory and Analysis of Available Data. *Atmos. Environ., Part A* 1992, *26* (6), 1071−1080.

(30) Brommer, S.; Jantunen, L. M.; Bidleman, T. F.; Harrad, S.; Diamond, M. L. Determination of Vapor Pressures for Organophosphate Esters. *J. Chem. Eng. Data* 2014, *59* (5), 1441−1447.

(31) Pankow, J. F. Review and Comparative-Analysis of the Theories on Partitioning between the Gas and Aerosol Particulate Phases in the Atmosphere. *Atmos. Environ.* 1987, *21* (11), 2275−2283.

(32) Wang, Z.; Na, G. S.; Ma, X. D.; Fang, X. D.; Ge, L. K.; Gao, H.; Yao, Z. W. Occurrence and gas/particle partitioning of PAHs in the atmosphere from the North Pacific to the Arctic Ocean. *Atmos. Environ.* 2013, *77*, 640−646.

(33) Lohmann, R.; Lammel, G. Adsorptive and absorptive contributions to the gas-particle partitioning of polycyclic aromatic hydrocarbons: State of knowledge and recommended parametrization for modeling. *Environ. Sci. Technol.* 2004, *38* (14), 3793−3803.

(34) Harner, T.; Bidleman, T. F. Octanol-air partition coefficient for describing particle/gas partitioning of aromatic compounds in urban air. *Environ. Sci. Technol.* 1998, *32* (10), 1494−1502.

(35) Wang, Q.; Zhao, H.; Wang, Y.; Xie, Q.; Chen, J.; Quan, X. Determination and prediction of octanol-air partition coefficients for organophosphate flame retardants. *Ecotoxicol. Environ. Saf.* 2017, *145*, 283−288.
(36) Sühring, R.; Diamond, M. L.; Scheringer, M.; Wong, F.; Pucko, M.; Stern, G.; Burt, A.; Hung, H.; Fellin, P.; Li, H.; Jantunen, L. M. Organophosphate Esters in Canadian Arctic Air: Occurrence, Levels and Trends. *Environ. Sci. Technol.* 2016, *50* (14), 7409−7415.
(37) Salamova, A.; Hermanson, M. H.; Hites, R. A. Organophosphate and Halogenated Flame Retardants in Atmospheric Particles from a European Arctic Site. *Environ. Sci. Technol.* 2014, *48* (11), 6133−6140.
(38) Li, C.; Chen, J.; Xie, H. B.; Zhao, Y.; Xia, D.; Xu, T.; Li, X.; Qiao, X. Effects of Atmospheric Water on.OH-initiated Oxidation of Organophosphate Flame Retardants: A DFT Investigation on TCPP. *Environ. Sci. Technol.* 2017, *51* (9), 5043−5051.
(39) Gao, Y.; Arimoto, R.; Duce, R. A.; Lee, D. S.; Zhou, M. Y. Input of Atmospheric Trace-Elements and Mineral Matter to the Yellow Sea during the Spring of a Low-Dust Year. *J. Geophys. Res.* 1992, *97* (D4), 3767−3777.
(40) Wang, R. M.; Tang, J. H.; Xie, Z. Y.; Mi, W. Y.; Chen, Y. J.; Wolschke, H.; Tian, C. G.; Pan, X. H.; Luo, Y. M.; Ebinghaus, R. Occurrence and spatial distribution of organophosphate ester flame retardants and plasticizers in 40 rivers draining into the Bohai Sea, north China. *Environ. Pollut.* 2015, *198*, 172−178.